Biomaterials Science

ROYAL SOCIETY OF CHEMISTRY

Check for updates

Gellan Gum-based luminal fillers for peripheral nerve regeneration: an *in vivo* study in the rat sciatic nerve repair model†

C. R. Carvalho, [a,b] S. Wrobel, [c] C. Meyer, [c] C. Brandenberger, [d] I. F. Cengiz, [a,b] R. López-Cebral, [a,b] J. Silva-Correia, [a,b] G. Ronchi, [e] R. L. Reis, [a,b,f] C. Grothe, [c] J. M. Oliveira *[a,b,f] and K. Haastert-Talini [c]

Peripheral nerve injuries (PNI) resulting in a gap to be bridged between the transected nerve ends are commonly reconstructed with autologous nerve tissue, but there is a need for valuable alternatives. This experimental work considers the innovative use of the biomaterial Gellan Gum (GG) as a luminal filler for nerve guidance channels made from chitosan with a 5% degree of acetylation. The engineered constructs should remodel the structural support given to regenerating axons by the so-called bands of Büngner. Four different GG formulations were produced by combining varying amounts of High-Acyl GG (HA-GG) and Methacrylated GG (MA-GG). The effective porosity of the freeze-dried networks was analysed by SEM and micro-CT 3D reconstructions, while the degradation and swelling abilities were characterized *in vitro* for up to 30 days. The metabolic activity and viability of immortalized Schwann cells seeded onto the freeze-dried networks were also evaluated. Finally, the developed hydrogel formulations were freeze-dried within the chitosan nerve guides and implanted in a 10 mm rat sciatic nerve defect. Functional and histomorphological analyses after 3, 6, and 12 weeks *in vivo* revealed that although it did not result in improved nerve regeneration, the NGC25:75 formulations could provide a basis for further development of GG scaffolds as luminal fillers for hollow nerve guidance channels.

1. Introduction

Peripheral nerves originate with their motor and sensory roots from the spinal cord or the brain stem, sending efferent signals from the Central Nervous System (CNS) to all organs and tissues, where they also collect afferent information and transmit it back to the CNS. Their widespread presence and lack of protection against transection or injuries make them vulnerable to diverse types of lesions, *i.e.* car accidents, military and sports injuries or metabolic damage. Indeed, peripheral nerve injuries (PNIs) affect over one million people across the world every year.[1] Although the peripheral nervous system (PNS) has a superior capacity to regenerate when compared to the CNS, this ability is not as efficient as desired and surgical intervention is often required. However, even if skilled microsurgical reconstruction is performed, inefficient recovery is common, leading to motor and sensory perception impairments, as well as very painful conditions.[2]

For PNIs that require surgical intervention, like all complete transection injuries, end-to-end suturing is applicable in the case of gaps shorter than 5 mm. For longer gap injuries autologous nerve grafts (AUTOGs) have been considered the gold standard for decades.[3] However, they are associated with several drawbacks, for instance, donor site morbidity and limited availability of donor tissue. Nerve mismatches are frequent, both in terms of size and alignment. Additionally, complete recovery of nerve function is rare. Meanwhile, immune rejection dismisses primary allografts and xenografts.[4] Nerve guidance conduits (NGCs), with base on the natural biology of regeneration, seem a potentially outstanding alternative to overcome this public health problem.[1,5,6]

a3B's Research Group – Biomaterials, Biodegradables and Biomimetics, University of Minho, Headquarters of the European Institute of Excellence on Tissue Engineering and Regenerative Medicine, AvePark – Parque de Ciência e Tecnologia, Zona Industrial de Gandra, 4805-017 Barco, Guimarães, Portugal. E-mail: miguel.oliveira@dep.uminho.pt
bICVS/3B's – PT Government Associated Laboratory, Braga/Guimarães, Portugal
cInstitute of Neuroanatomy and Cell Biology, Hannover Medical School, Hannover, Germany and Center for Systems Neuroscience (ZSN), Hannover, Germany
dInstitute of Functional and Applied Anatomy, Hannover Medical School, 30625 Hannover, Germany
eDepartment of Clinical and Biological Sciences, and Cavalieri Ottolenghi Neuroscience Institute, University of Turin, Turin, Italy
fThe Discoveries Centre for Regenerative and Precision Medicine, Headquarters at University of Minho, Avepark, 4805-017 Barco, Guimarães, Portugal
†Electronic supplementary information (ESI) available. See DOI: 10.1039/c7bm01101f

To date, several NGCs have been developed, using many different strategies, from simple hollow tubes[7,8] to subdivided or filled tubes,[9,10] also comprising the addition of neurotrophic factors[11,12] or stem cells.[13,14] Also, their combinations were explored.[15]

FDA approved NGCs consist of hollow tubular structures, made from cross-linked collagen, resorbable biopolymers or non-resorbable hydrogels.[16] The absence of luminal structures to guide axons and Schwann cells, the peripheral glia cells, was pointed out to be one possible cause for their failure in long gap PNIs.[17,18]

Chitosan is a polysaccharide extracted mainly from crab shells and has been widely studied owing to its application in nerve regeneration.[19] Recently, Reaxon® (Medovent GmbH, Germany), a nerve guide made from chitosan with a 5% degree of acetylation,[20] received CE and FDA approval for reconstruction of up to 26 mm in length peripheral nerve defects in humans. Current research efforts focus on the design of more refined chitosan nerve guides able to support the reconstruction of nerve defects exceeding 3–5 cm in length. Consequently, luminal enrichment should be further engineered to optimize axonal guidance. The strategies already explored range from simply inserting a central longitudinal chitosan film[9] to adding regenerative hydrogel matrices, like a hyaluronic acid and laminin based hydrogel.[21]

Gellan Gum (GG) is a linear anionic polysaccharide composed of tetrasaccharide (1,3-b-D-glucose, 1,4-b-D-glucuronic acid, 1,4-b-D-glucose, 1,4-a-L-rhamnose) repeating units. This biomaterial exists in nature in two forms: a high-acyl (HA-GG) and a low-acyl (LA-GG) forms. The side groups in the LA-GG polymeric chain are susceptible to chemical modification, such as the incorporation of methacrylate groups (MA-GG). The methacrylation process allows harsh reagent-free hydrogel preparation, with temperatures and pH resembling those of the human body.[22]

This experimental work proposes the utilization of different HA-GG and MA-GG blending hydrogels as luminal fillers of tubular chitosan nerve guidance conduits (NGC). Since HA-GG and MA-GG behave differently, these blends are expected to affect the hydrogel degradation rate and cellular adhesion, thus permitting determining the influence of these parameters on the peripheral nerve regeneration process. To our knowledge, this is the first time that the biomaterial GG was studied with regard to PNR purposes. However, GG has already shown great potential for other regenerative applications, such as dentistry,[23] fibrocartilage tissue engineering,[24] wound healing[25] or bone regeneration,[26] as well as in the area of drug delivery.[27,28] After the production of different GG formulations, the hydrogels were subjected to a physicochemical characterization and *in vitro* preliminary assessment using immortalized Schwann cells. Subsequently, the formulations were injected into chitosan nerve guidance conduits, freeze-dried and implanted *in vivo* for different periods of observation time. Immunohistochemical studies were carried out to assess nerve regeneration and re-vascularization, allied to macroscopic evaluation of the explants, and evaluation of functional motor

recovery and nerve morphometry. The evaluation of their characteristics was performed in a 10 mm sciatic nerve defect in order to select the most promising as a luminal filler for NGCs for future studies in longer gaps.

2. Materials and methods

2.1 Production of biomedical systems

2.1.1 Production of Gellan Gum freeze-dried hydrogels. Four different GG-based formulations were obtained by combining 0.7% (w/v) HA-GG (KelcoGelW LT100 with MW = 1–2 × 106 Da, CP Kelco, Atlanta, GA, USA) and 0.7% (w/v) MA-GG (Mimsys G® with MW = 62.4 kDa, Stemmatters, Irisbiosciences,12 Guimarães, Portugal) aqueous solutions. The studied ratios were 60 : 40%, 50 : 50%, 25 : 75%, and 0 : 100% (v/v) HA-GG : MA-GG (see Table 1). These preparations were heated at 37 °C for 30 minutes and transferred into silicone disc moulds (diameter and height were 6 mm and 10 mm, respectively) self-made from silicon tubing (purchased from Deltalab, Spain), which were ultimately immersed in PBS solutions (pH = 7.4) overnight. Gelation occurred by ionic crosslinking at room temperature (RT). These hydrogels were punched with a branched (200 μm diameter linear branches) metallic self-made device (stainless steel) in order to create interior linear porous channels. The obtained hydrogels were frozen (−80 °C) and freeze-dried. The polymeric networks obtained will be transformed into hydrogels after rehydration.

2.1.2 Production of chitosan nerve guidance conduits (NGCs) filled with freeze-dried Gellan Gum hydrogels. Chitosan hollow tubes, kindly supplied by Medovent GmbH (Mainz, Germany), were manufactured under ISO 13485 conditions using Medical grade chitosan (*Ki2*Med® LO_{80+} extracted from *Pandalus borealis* shrimp shells, MW = 260 kDa, supplied by Altakitin S. A., Lisbon, Portugal). More specifically, an extrusion process was applied for obtaining them, followed by distinctive washing and hydrolysis steps to set the Degree of Acetylation at a 5% value. The formulations were finally cut into fragments of the required length (14 mm) and sterilized by ethylene oxide. The mixtures mentioned in section 2.1.1. (60 : 40%, 50 : 50% and 25 : 75% (v/v) HA-GG : MA-GG) were injected inside the tubes with the help of a syringe. During this step, it was important to keep 2 mm hydrogel-free segments at each extreme of the tube, for nerve insertion and

Table 1 Gellan Gum formulations and designations. This table presents the nomenclature utilized to designate the different formulations studied during this experimental work

Composition	Freeze-dried hydrogel formulation	NGC (freeze-dried hydrogel filling chitosan tube)
60 : 40% (v/v) HA-GG : MA-GG	H60:40	NGC60:40
50 : 50% (v/v) HA-GG : MA-GG	H50:50	NGC50:50
25 : 75% (v/v) HA-GG : MA-GG	H25:75	NGC25:75
0 : 100% MA-GG (v/v) HA-GG : MA-GG	H0:100	x

suture purposes. The filled tubes were then immersed in PBS overnight for gelation by ionic crosslink, frozen at −80 °C and freeze-dried (see Table 1).

2.2 Physicochemical characterization

2.2.1 Microstructure evaluation. The microstructure evaluation was performed by means of observation in a stereomicroscope, in a Scanning Electron Microscope (SEM), and X-ray micro-computed tomography (micro-CT) analysis. The freeze-dried HA-GG : MA-GG hydrogel formulations and HA-GG : MA-GG hydrogel filled chitosan NGCs (Table 1) were examined under the Stereo Microscope + Lamp (Schott KL 200, model Stemi 1000, Zeiss). For SEM, the formulations described were sputter coated with gold in order to facilitate the analysis of their surface morphology (model S360, Leica, Cambridge, England). The microstructure of the formulations was also qualitatively and quantitatively evaluated by micro-CT analysis (n = 3). The detailed structure of the samples was acquired by X-ray scanning and 3D-reconstructed. Morphometric parameters, such as porosity, mean pore size and trabecular thickness, were determined. Data acquisition was carried out using a SkyScan 1072 scanner with a pixel size of 2 μm and an integration time of 1182 ms. The X-ray source was set at 39.4 kV and 244 μA. A total of 500 projections were acquired over a rotation range of 180°, with a rotation step of 0.23°. Datasets were reconstructed using standardized cone-beam reconstruction software (NRecon v. 1.6.6.0, SkyScan). The output format for each sample was bitmap images. The set of images was orientated with DataViewer software (v. 1.4.4, SkyScan) to obtain all the samples in the same axis. A representative dataset of the slices was segmented into binary images with a dynamic threshold of 40–120, which were used for morphometric analysis (CT Analyser, v. 1.12.0.0, SkyScan) and to obtain the 3D models (CT Vox, v. 2.3.0 r810, SkyScan).

2.2.2 Water uptake and weight loss. Water uptake and weight loss studies concerning the GG freeze-dried hydrogels were performed by means of PBS (pH 7.4 at 37 °C) soaking. At predefined time points (1, 7, 14 and 30 days) swollen or degraded samples were extracted and excess water removed with filter paper. The water uptake ability of the formulations was calculated according to eqn (1). To determine the degradation profile over time the samples were dried at RT and eqn (2) was applied.

$$\text{Water uptake } (\%) = (MW - MI)/MI \times 100, \qquad (1)$$

where MW is the Wet Mass (after excess water removal) and MI is the Initial Mass.

$$\text{Weight loss } (\%) = (MI - MF)/MI \times 100, \qquad (2)$$

where MI is the Initial Mass (before immersion in solution) and MF is the Final Mass (after drying).

Three replicates of each sample were studied and the average values were considered.

2.3 Biological *in vitro* assays

Rat immortalized Schwann cells (iSCs)[29] were taken from a stock and cultured in non-coated cell culture flasks. The culture medium was DMEM supplemented with 10% foetal calf serum, 1% Penicillin/Streptomycin, 1% sodium pyruvate, and 1% L-glutamine (all from PAA Laboratories GmbH).

2.3.1 Metabolic activity evaluation. iSC metabolic activity was followed using Alamar Blue (AB), a dye that yields a fluorescent signal and a colorimetric change when incubated with metabolically-active cells. The cells were directly seeded (500 000 cells per scaffold) over the GG freeze-dried hydrogels. After 1, 5 and 7 days *in vitro* (DIV), a specific cell culture medium containing 10% AB was added to the different culture wells. The systems were left for incubation for 3 hours, after which the fluorescence was monitored at 590 nm emission wavelength (excitation wavelength 530 nm) using a microplate reader (FL 600, Bio-Tek Instruments). AB reagent was removed using PBS and fresh culture medium was added in its place after each AB determination. The metabolic activity values were calculated by normalization with the mean fluorescence value obtained for the negative controls (different formulations without cells that undergo the exact same processing). The positive control refers to the same cellular density seeded on tissue culture polystyrene (TCPs).

2.3.2 Live/dead viability assay. iSC viability was qualitatively assessed using Calcein AM (for living cells) and propidium iodide staining (for dead cells). The cells were seeded (500 000 cells per scaffold) over the dry network formulations. After 1, 5 and 7 days *in vitro* (DIV), each scaffold was washed with PBS and immersed in 1 mL of culture medium supplemented with 2 μg Calcein AM and 4 μg propidium iodide (Life Technologies, CA, USA). These immersions lasted for 2 hours, after which the samples were thoroughly washed with PBS. The samples were analyzed using a transmitted and reflected light microscope (Axio Imager Z1m, Zeiss, Jena, Germany).

2.4 *In vivo* study

2.4.1 Experimental design. The effectiveness of the developed chitosan tubes filled with freeze-dried hydrogels as PNR guidance conduits (see Table 1; NGC60:40, NGC50:50 and NGC25:75) was tested in a 10 mm rat sciatic nerve defect. Samples for histological analysis were collected after both short-term (ST, 3 and 6 weeks) and long-term (LT, 12 weeks) observation periods. For the ST studies, 4 animals were selected for the implantation of each NGC formulation. Hollow chitosan tubes served as positive controls.[20] For LT studies, 7 animals were studied per NGC formulation and 7 animals receiving an autologous nerve graft (AUTOG) served as controls. The majority of the *in vivo* studies described in this experimental work were performed in Hannover Medical School (MHH, Hannover, Germany), except for the micro-CT analysis of the explants and vascularization detection studies, which were performed in 3B's Research Group (Guimarães,

Portugal). Histomorphometry was completed at University of Turin (UNITO, Italy).

2.4.2 Surgical procedure.

All animal experiments followed the rules of the EU Directive 2010/63/EU for animal experiments and were permitted by the animal care committee of Lower-Saxony, Germany: Nds. Landesamt für Verbraucherschutz und Lebensmittelsicherheit Dezernat 33/Tierschutz, reference number 33.12 42502-04-12/0816.

Female Wistar rats (225 to 250 g) were kept in groups of four animals under standard conditions (room temperature 22 ± 2 °C; humidity 55 ± 5%; light–dark cycle 14 h/10 h), with food and water *ad libitum*. For surgical procedures, animals were anesthetized by an intraperitoneal injection of chloral hydrate (370 mg kg^{-1} of body weight, Sigma-Aldrich). NGCs with a length of 14 mm were saturated for 30 minutes in 0.9% NaCl prior to implantation. Animals were placed on a thermostatic blanket throughout the surgical procedures and postoperative periods. Aseptic conditions were observed.

After exposure of the sciatic nerve, it was transected at a constant point (6 mm from the exit of the gluteus muscle) for the removal of 5 mm of the distal end. Once the PNI was caused, NGCs were implanted to bridge a 10 mm nerve defect. NGCs were connected by a single 9-0 suture (9-0, EH7981G, Ethilon, Ethicon, Scotland) to the respective nerve end. Alternatively, autologous nerve grafts were implanted. Therefore, a 10 mm nerve segment was excised from the same nerve (proximal transection again at 6 mm from the exit of the gluteus muscle), reversed and 180° turned along its longitudinal axis, and sutured back into the nerve with three 9-0 sutures at each end. Postoperative analgesia was guaranteed by intramuscular injection of buprenorphine (0.045 mg kg^{-1} of body weight, Buprenovet®; Bayer Pharmaceuticals, Leverkusen, Germany).

2.4.3 Evaluation of functional motor recovery.

Electrodiagnostic recordings of evoked compound muscle action potentials (CMAPs) from the anterior tibial muscles (TA) and the plantar muscles (PL) were performed. During the 12 week study period two sessions of non-invasive (week 4 and week 8 post-surgery) measurements and one final session of invasive (12 weeks post-surgery) measurements were carried out. The investigators performing the tests were blinded for the general implantation conditions and the formulation type of the implanted tubes.

In brief, a portable electrodiagnostic device (Keypoint Portable; Medtronic Functional Diagnostics A/S, Denmark) was used to stimulate the sciatic nerve and to record the evoked CMAPs. In the non-invasive setting, the sciatic nerve was stimulated with single electrical pulses (100 µs duration and supramaximal intensity) delivered by monopolar needles (30G, diameter 0.3 mm, length 10 mm; Natus Europe GmbH, Planegg, Germany), percutaneously placed at the sciatic notch (proximal stimulation) or at the popliteal fossa (distal stimulation). The active recording electrode was located in the respective muscle belly, the reference electrode in the tip of the second toe and the ground needle electrode was inserted in the skin at the flank. In the invasive setting, the sciatic

nerves at both the injured and non-injured sides were consecutively exposed. With the help of a bipolar steel hook electrode, the sciatic nerves were directly stimulated proximal and distal to the transplants. Single electrical pulses (100 ms duration) with gradually increased intensity (not exceeding 8 mA) were applied in order to evaluate the threshold and maximal CMAP. The recording electrodes were placed as described before. Whenever a CMAP could be evoked, the signal was recorded and the signal amplitude of the negative CMAP peak analysed. Amplitude ratio values were obtained using CMAP signals evoked and recorded from the contralateral healthy side of the animal. If no evoked CMAP was detected, a 0.00 value was noted down.

2.4.4 Macroscopic inspection of the reconstructed nerves upon explantation.

At the end of the ST or LT observation periods, animals were sacrificed under deep general anaesthesia, following the animal protection rules. The regenerated sciatic nerves were exposed and inspected with the help of a microsurgery microscope.

2.4.5 Micro-CT evaluation of the explants.

This technique was performed in 3B's Research Group (Guimarães, Portugal) after shipment of the entire LT study (12 weeks) explants from MHH (Hannover, Germany) which were preserved in ethanol solutions.

The explants were scanned using a high-resolution micro-CT device, VivaCT 80 (Scanco Medical AG, Brüttisellen, Switzerland). 250 projections with a resolution of 1024 × 1024 pixels were obtained in each scan with an integration time of 200 ms. Images with an isotropic pixel size of 31.2 µm were obtained at 45 kV, 177 µA and 8 W. The acquired images were reconstructed to obtain 2D image datasets in µCT Evaluation Program V6.5 (Scanco Medical AG, Brüttisellen, Switzerland). Using the CT Analyser software V1.15.4.0 (Bruker micro-CT, Belgium) the regions of interest were defined on the 2D images of the explants that were viewed in 3D and 2D all planes on DataViewer V1.5.3.6 (Bruker micro-CT, Belgium).

2.4.6 Nerve histology for detection of axonal regeneration and immunological reaction‡.

After the corresponding period of study, the animals were sacrificed and the nerve implants, together with the respective controls, were harvested for further analysis. The entire samples were fixed in 4% PFA overnight (4 °C), transferred to 70% ethanol and subsequently embedded in paraffin.‡

For both, 6 weeks and 12 weeks time point samples, longitudinal sections were produced in order to harvest the complete length of the GG material and eventually regrown tissue along the 10 mm nerve gap. As soon as the complete length of the material was visible in one section, a series of 24 sections (7 µm thickness) was produced and two sections per slide were collected. Again, the sections on one slide were harvested at

---

‡During the ST study, explanted samples were, immediately after explantation and macroscopic evaluation, processed for histology. In contrast, samples obtained after the LT observation period were sent back from 3B's Research Group (Guimarães, Portugal) to MHH (Hannover, Germany) after micro-CT scanning in order to have them processed for histology.

84 μm distance from each other. Once the first section series was completed a similar one, the second one, was collected without discarding any tissue. In the end, a total distance of 336 μm was longitudinally cut from the middle of the NGC content.

Selected slides were subjected to haematoxylin–eosin (HE) staining. Briefly, samples were deparaffinised in xylol, hydrated through decreasing ethanol series (100%, 96%, 70% and 50% alcohol) and finally washed in distilled water. After immersion in haematoxylin, samples were rinsed in running soft tap water. Samples were then immersed in an 80% alcohol solution and briefly in the eosin staining. Slides were dehydrated through 96% ethanol, absolute ethanol and finally cleared in xylol and mounted with Moviol (Calbiochem, Germany, No. 475904).

Immunohistology was performed over sections that were consecutive to the ones processed for HE staining. A double-staining was performed to detect neurofilaments (NF-200) and activated macrophages (ED-1). Nuclear counterstaining was obtained with DAPI. For such, slides were deparaffinised and immersed in an antigen retrieval solution (citrate buffer, 10 mM, pH 6.0 + 0.05% Tween 20), heated at 90 °C for 30 minutes and left to cool down for another 30 minutes in distilled water. Afterwards, they were incubated in a blocking solution (PBS + 5% milk powder + 0.5% Triton X-100) prior to incubation with a primary mouse anti-rat ED-1 antibody (1 : 1000 diluted in blocking solution, MCA 275R Serotec, UK) at 4 °C overnight. The next day the sections were washed with PBS (3×) before being incubated with an Alexa 555-conjugated secondary goat-anti-mouse antibody (1 : 1000 diluted in blocking solution, Invitrogen, Germany) for 1 hour at room temperature (RT). After incubation with the secondary antibody, sections were further washed with PBS (3×) and a second blocking step was performed for 20 minutes.

Overnight incubation (4 °C) with a primary rabbit anti-rat NF-200 antibody (1 : 200 diluted in blocking solution, N4142, Sigma Aldrich, Germany) was done following the previously described steps. The samples were washed with PBS (3×) and incubated with an Alexa 488-conjugated secondary goat-anti rabbit antibody (1 : 1000 diluted in blocking solution, Invitrogen, Germany) for 1 hour at RT. The double-labelled sections were afterwards counterstained with the nuclear dye (DAPI, 1 : 2000 diluted in PBS, Sigma, Germany) for 5 minutes at RT, and finally mounted with Moviol.

For the qualitative analysis, representative photomicrographs of HE stained sections were taken with the help of BX53 and BX51 microscopes, as well as analysed with the help of the programs CellSense Dimension and CellSense Entry (all from Olympus, Germany). Immunohistochemistry images were digitized by means of a fluorescence microscope (BX60, Olympus, Germany), operated by using cellP software (Olympus, Germany) and also qualitatively analysed.

2.4.7   Nerve histology for the detection of neovascularization‡. Immunohistology for neovascularization (CD31 and CD34) was performed in 3B's Research Group (Guimarães, Portugal), after shipment of paraffinised slides. Slide sections consecutive to the ones processed for HE and double immuno-staining staining were used for this purpose. Blind-coded sections from each segment were deparaffinised and immersed in an antigen retrieval solution (citrate buffer, 10 mM, pH 6.0 + 0.05% Tween 20), heated at 90 °C for 30 minutes and left to cool down for another 30 minutes in distilled water. Slides were posteriorly immersed in a blocking solution (PBS + 3% BSA) prior to incubation with a primary goat anti-Mouse/Rat CD31/PECAM-1 antibody (AF3628, R&D Systems, UK) (15 μg ml^{-1} diluted in PBS + 1% BSA) at 4 °C overnight. The next day the corresponding sections were washed with PBS (3×) before being incubated with an Alexa 488-conjugated secondary rabbit anti-goat antibody (1 : 500 in PBS + 1% BSA) for 1 hour at RT. After incubation with the secondary antibody, sections were further washed with PBS (3×) and a second blocking step was done for 20 minutes. This was followed by overnight incubation (4 °C) with a primary rabbit anti-mouse CD34 antibody (1 : 2500 diluted in PBS + 1% BSA, Abcam, Cambridge, UK). After washing with PBS (3×), incubation with an Alexa Fluor 594 donkey anti-rabbit IgG secondary antibody (1 : 500 diluted in PBS + 1% BSA, Molecular Probes, Oregon, United States) was performed for 1 hour at RT. Sections were finally counterstained with the nuclear dye (DAPI, 1 : 2000 diluted in PBS, Sigma, Germany) for 5 minutes at RT and then mounted with PermaFluor (Thermo Fisher Scientific, UK). Since for the 3 weeks' time point the samples were cut into cross-sections, the example photo belongs to an area around 5 mm after the proximal nerve end. Results were qualitatively analysed using a transmitted and reflected light microscope (Axio Imager Z1m, Zeiss, Jena, Germany).

2.4.8   Nerve morphometry. In the LT study, upon explantation 12 weeks after nerve reconstruction, nerve tissue segments 5 mm in length were harvested directly distal to the sutures connecting the implants with the distal nerve end and processed for nerve morphometry. Segments taken from the contralateral healthy nerve at a similar height served as controls. Therefore, fixation was performed in Karnovsky fixans (2% PFA, 2.5% glutaraldehyde in 0.2 M sodium cacodylate buffer, pH 7.3, for 24 h)[30,31] prior to rinsing the samples 3 times with 0.1 M sodium cacodylate buffer containing 7.5% sucrose. Post-fixation was performed in 1% OsO$_4$ for 1.5 hours followed by myelin staining for 24 h in 1% potassium dichromate, 24 hours in 25% ethanol and 24 h in hematoxilin (0.5% in 70% ethanol), according to a modified Schultze protocol.[32] After dehydration, the samples were embedded in EPON (SERVA Electrophoresis GmbH, Heidelberg, Germany). Semi-thin (1 μm) cross-sections were cut with glass knives (Ultramikrotome System, 2128 Ultrotome®, LKB, Bromma, Sweden) and mounted on uncoated glass slides. Toluidine blue staining was then performed to further enhance the myelin staining.[33] For quantitative analysis, those samples were chosen that were obtained from animals with electrodiagnostically proved reinnervation of the tibialis anterior muscle 12 weeks after surgery (LT). Morphometric analysis revealed the total number of myelinated fibers, cross sectional area, nerve fiber density, axon diameter, fiber diameter, g-ratio, and

myelin thickness. All histomorphometry was performed with the help of systematic random sampling[20] at the University of Turin (UNITO, Italy) after shipping the finalized slides/sections from MHH.

2.5 Statistical analysis

All quantitative physicochemical and biological *in vitro* experiments were run in triplicates, and the results are expressed as the mean ± standard deviation. Statistical analysis of the data was conducted using GraphPad Prism Software for Windows, version 5.00 (GraphPad Software, Inc., La Jolla, USA). Regarding the Alamar Blue assay, normality of the data distribution was tested by using the Shapiro–Wilk normality test. Afterwards, a Kruskal–Wallis test was performed in order to compare the different groups, followed by Dunn's multiple comparison test. The significance level was set at $*p < 0.05$, $**p < 0.01$, and $***p < 0.001$.

No statistical analysis was performed on the data obtained during functional evaluation of nerve recovery since $n \leq 3$ of the NGC groups demonstrated functional recovery and the numbers were too few for statistical analysis. The results of the morphometric analysis are given in terms of the mean ± SD for healthy nerve samples, AUTOG and NGC25:75, while for less than 3 animals per group (NGC50:50) the single values are presented. $*p < 0.05$ after Dunn's multiple comparison test.

3. Results

3.1. Physicochemical characterization

3.1.1 Microstructure evaluation. All GG freeze-dried hydrogels (H60:40, H50:50, H25:75, H0:100, Table 1) were analysed according to the techniques mentioned above. However, due to the similar aspects of the different formulations, only the images corresponding to formulation H25:75 are presented.

In Fig. 1, the first row of images shows the different representative aspects displayed by GG formulations along the preparation process. Fig. 1A presents an outline of the network with the intended microstructure. Fig. 1B shows the hydrogels obtained after the ionic PBS cross-linking. These hydrogels were punched with branched wires (Fig. 1C) to produce vertical aligned porous channels within their structure. Fig. 1D shows the aspects of the freeze-dried networks obtained. Once rehydrated with cell culture medium, the formulations become hydrogels that maintain the conferred porous structure (Fig. 1E). Fig. 1F shows the SEM microphotographs corresponding to the surfaces of the cross-sections. High diameter pores (around 200 μm) can be seen, which originate from both, metallic punching and freeze-drying. Meanwhile, Fig. 1G presents the longitudinal cut of a scaffold. The aligned channels made by the metallic device (indicated by arrows) are clearly discernible from the random pores obtained by freeze-drying. Fig. 1H and I show the longitudinal and transversal sections, respectively, of the chitosan tubes (arrows pointing to their walls) filled with the GG freeze-dried hydrogels.
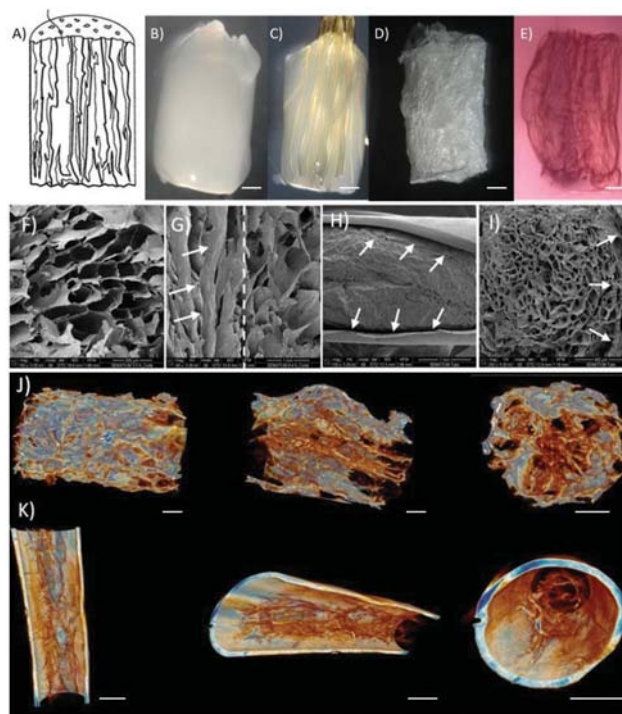

Fig. 1 Macro- and microstructure evaluation of the developed formulations. The first row of images corresponds to the different aspects of the formulations throughout the production process: (A) scheme of a scaffold with the intended microstructure of vertically aligned channels; (B) hydrogels obtained after the ionic PBS cross-linking; (C) hydrogels punched with branched wires to display longitudinal porous channels; (D) freeze-dried hydrogels; (E) rehydrated freeze-dried hydrogels resembling the initial scheme. The second row of images corresponds to SEM micrographs of the freeze-dried formulations: (F) surface cross-section of the scaffold; (G) longitudinal cut of the scaffold. White arrows point to the aligned channels made by the punching (right), which differ from the random network porosity (left); (H) longitudinal section of a chitosan NGC (arrows pointing to the wall of it) filled with GG freeze-dried hydrogels and (I) cross-section of the chitosan NGC (arrows pointing to its wall) filled with GG freeze-dried hydrogels. The third row of images reveals the structure of the biomaterials after micro-CT 3D reconstructions: (J) 3D reconstructions of freeze-dried GG networks; (K) 3D reconstructions of final NGC constructs. As the aspects of all the studied formulations are very similar, the previously presented images are representative of all of them. Scale bars: 1 mm.

Micro-CT studies were performed to obtain 3D reconstructions of the studied formulations at the micrometric level. Fig. 1J and K show the 3D reconstructed structures of the freeze-dried GG hydrogels and the final NGC constructs, respectively.

Micro-computed tomography technology was also used to define the mean pore size (μm), the mean trabecular thickness (μm) and the % of porosity of all developed formulations. Regarding the freeze-dried GG formulations, detailed results can be found in the supplementary material supplied (ESI Table S1†). The mean pore size varied from 230.6 ± 3.2 to 339.0 ± 75.9 μm, trabecular thickness from 58.1 ± 2.1 to 65.8 ± 4.7 μm and the % of porosity from 79.2 ± 1.7 to 81.5 ± 8.2%. For hydrogels freeze-dried within NGCs (ESI Table S2†) the
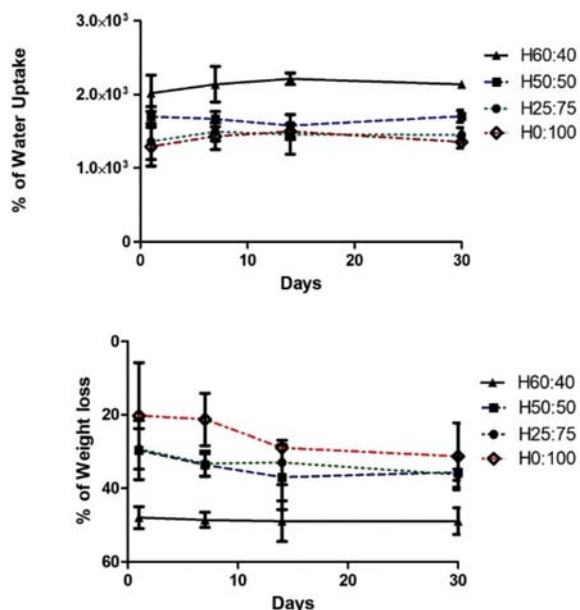
Fig. 2 Percentage of water uptake and weight loss of the developed GG freeze-dried hydrogels. The graphics present the water uptake and weight loss values corresponding to all the studied formulations along the 30 days of study. The evaluations were performed at 37 °C.

mean pore sizes varied from 321.6 ± 89.4 to 377.8 ± 50.8 μm, trabecular thickness from 98.0 ± 13.5 to 121.4 ± 13.4 μm and the % of porosity from 73.8 ± 7.3 to $82.8 \pm 5.2\%$.

3.1.2 Water uptake and weight loss. The results of water uptake (WU) and weight loss (WL) can be seen in Fig. 2. With respect to WU, all of the studied formulations reached maximum swelling stability after 1 day of immersion. From that day to day 30 the percentages of swelling were more or less constant. H60:40 is the formulation with higher WU, presenting values slightly above 2000%. In contrast, H0:100% is the system having lower WU, with values reaching 1000%. The H60:40 formulation showed a higher mass loss (around 45%) when compared to the other formulations. In contrast, H0:100% formulations underwent the lowest WL, as the loss reached an average of 20 to 30% of mass after 30 days.

3.2 Biological *in vitro* assays

3.2.1 Metabolic activity of immortalized Schwann cells. The results (Fig. 3A) show a general increase in the metabolic activity on increasing the amounts of MA-GG in the formulations, regardless of the time point analysed, the highest values were obtained for H0:100. However, in general, the metabolic activity values did not increase significantly over
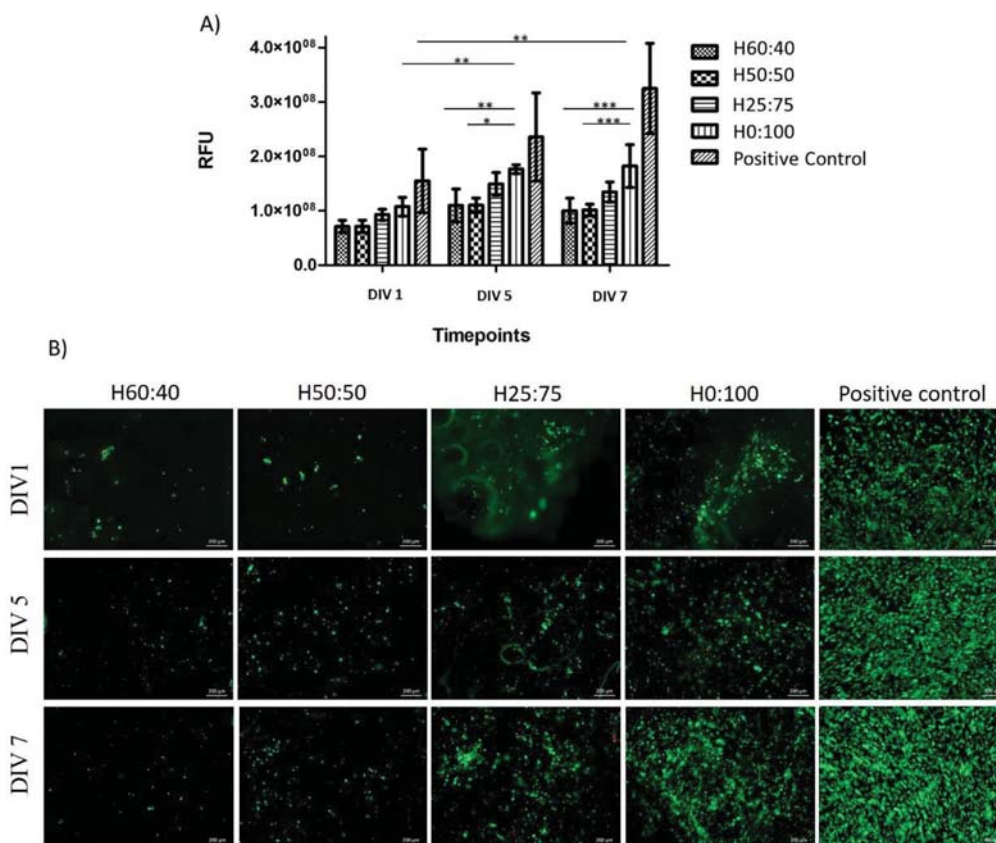

Fig. 3 Biocompatibility of GG formulations with immortalized Schwann cells (iSCs) *in vitro*. (A) Metabolic activity of iSCs seeded on freeze-dried hydrogel formulations after up to 7 days; determination by Alamar Blue; $n = 3$. (B) Representative Live/Dead qualitative assay images after direct iSC seeding on freeze-dried hydrogel formulations after up to 7 days; determination by Calcein AM (green fluorescence) and propidium iodide (red fluorescence). Scale bars: 200 μm.

time. The only exception was formulation H0:100%, with a significant increase in metabolic activity both from day 1 to 5 and from day 1 to 7. Indeed, both at 5 and 7 days the metabolic activity of iSCs seeded onto the H0:100% formulation was significantly higher than that obtained from iSCs on H60:40 and H50:50.

3.2.2 Live/dead viability assay. In Fig. 3B it can be seen that, in accordance with the metabolic activity quantification, an increasing number of living cells are present in the formulations with the increase in the amount of methacrylated GG, from H60:40 to H0:100. As expected, the number of living cells also increases progressively with time (days *in vitro*). Importantly, the number of dead cells is negligible, as reflected by the presence of very few red-stained spots.

3.3 *In vivo* studies

A concise summary of all the results presented in the following paragraphs for the GG filled NGCs can be found in the ESI.† Wherever appropriate, the reader will be referred to Tables S4, S5 or S6† that summarize the results of an evaluation performed on samples retrieved 3 weeks, 6 weeks and 12 weeks after reconstruction, respectively. For the ST studies, hollow chitosan tubes served as positive controls[20] and 4 animals per group were selected for implantation of each NGC formulation. For LT studies, the autologous nerve graft (AUTOG) group served as controls and 7 animals were subjected each to implantation of either an NGC formulation or an AUTOG.

3.3.1 Evaluation of functional motor recovery. Functional nerve regeneration was only examined during the LT experiment (at 4, 8 and 12 weeks). Here, the recovery observed after implantation of NGCs filled with different freeze-dried GG formulations (n = 7 NGC60:40, n = 7 NGC50:50, n = 5 NGC25:75) was compared to that observed after implantation of AUTOGs (n = 7). In the following weeks, however, the number of animals in the NGC25:75 group was reduced by two in comparison with the other groups, because the animals had to be removed from the study after showing massive autotomy behaviour. The results of electrodiagnostic measurements are presented in Table 2. After 4 weeks of implantation there was no functional recovery. Consequently, the presented results correspond to 8 and 12 weeks post-implantation. After 8 weeks, only animals from the AUTOG group showed nerve recovery, represented by CMAPs recorded from the tibialis anterior (86%) or plantar muscles (43%) upon stimulation of the reconstructed sciatic nerve. At 12 weeks post-surgery, the control group (AUTOG) demonstrated an increased degree of recovery with 100% and 71% evocable CMAPs recorded from the tibialis anterior and plantar muscles, respectively.

Recovery in animals transplanted with GG-filled NGCs was less frequent. At that time point, nerve reconstruction with NGC60:40 did not result in any detectable muscle reinnervation. Only two animals from the NGC50:50 (29%) group and three animals from the NGC25:75 group (60%) displayed evocable CMAPs, which were also recordable only from the more proximal tibialis anterior muscle. The small number of

Table 2 Evaluation of functional motor recovery. This table presents the percentages, as well as animals per group, with evocable compound muscle action potentials (CMAPs) recordable from the tibialis anterior muscle or plantar interosseous muscle. The measurements were performed 4, 6 and 12 weeks after nerve reconstruction surgery. The varying animal numbers displayed for CMAP recordings from tibialis anterior and plantar muscles, respectively, are related to eventual temporary suspension of animals from plantar recordings upon the occurrence of signs of minimal autotomy

	8 weeks		12 weeks (invasive)	
	Animals/group	Percentage	Animals/group	Percentage
Tibialis anterior muscle				
AUTOG	6/7	86%	7/7	**100%**
NGC60:40	0/7	0%	0/7	**0%**
NGC50:50	0/7	0%	2/7	**29%**
NGC25:75	0/5	0%	3/5	**60%**
Plantar muscle				
AUTOG	3/7	43%	5/7	71%
NGC60:40	0/7	0%	0/7	**0%**
NGC50:50	0/3	0%	0/6	0%
NGC25:75	0/4	0%	0/5	0%

animals displaying motor recovery detectable by electrodiagnostic procedures did not justify any statistical analysis. However, as depicted in ESI Fig. S1,† a closer look at the CMAP amplitude ratios ($mV_{ipsilateral}/mV_{contralateral}$) revealed that the quality of regeneration in one animal of the NGC25:75 group ranged among the values also detected in the AUTOG group animals.

3.3.2 Macroscopic inspection of nerve implants. Since the chitosan NGC is transparent, macroscopic inspection of its content can be performed with the help of a microsurgery microscope. At 3 weeks post-surgery a tissue bridge connecting the nerve ends through the hollow NGCs of the control group were detectable in 4/4 cases, as expected from the positive control. At the same time, NGCs from the NGC60:40 group did not contain any visible tissue (0/4), while 1/4 NGC50:50 samples and 2/4 NGC25:75 samples displayed some (nerve) tissue infiltration of the GG scaffolds. ESI Fig. S2† shows photographs of representative samples harvested at 3 weeks post-surgery and ESI Table S4† summarizes the results of the macroscopic inspection of all samples.

At 6 weeks after surgery 3/4 NGCs from the control group (hollow chitosan NGCs) contained a visible tissue bridge connecting the nerve ends, while the last specimen from this group only contained a hairy connection, as it was not much thicker than a hair when inspected by the naked eye. Again, NGCs from the NGC60:40 group did not display visible ingrowth of nerve tissue into the GG scaffolds. However, the scaffolds appeared to be infiltrated by cells. At the same time 1/4 NGC50:50 samples and 3/4 NGC25:75 samples appeared to contain more organized (nerve) tissue. Residues of GG s could be clearly identified in the latter two groups as well. It is noteworthy that some of the samples demonstrated a clear vascularization of the NGC contents. ESI Fig. S3† shows photo-

graphs of representative samples harvested at 6 weeks post-surgery and ESI Table S5† summarizes the results of the macroscopic inspection of all samples.

At 12 weeks after surgery, all NGCs contained either residues of the freeze-dried GG hydrogel material or the same together with tissue infiltration. NGC contents frequently displayed a vascularization by small vessels grown longitudinally through the NGC. Compact nerve tissue, however, could not be clearly identified macroscopically. Implants were more closely inspected for which a content of regenerated nerve tissue could be expected after positive evaluation with electrodiagnostic procedures. This was the case for two samples from the NGC50:50 group and three samples from the NGC25:75 group. The NGC50:50 samples indicated from a macroscopic inspection that the regrown tissue had used the GG scaffolds as guidance structures. From the macroscopic inspection of the NGC25:75 samples it appeared that the regenerated tissue was more grown around or along the central GG scaffold instead of having the axons using the longitudinal channels within them as guidance structure. However, these impressions were put into another perspective after a histological evaluation of the samples as described below. ESI Fig. S4† shows photographs of representative samples harvested at 12 weeks post-surgery and ESI Table S6† summarizes the results of the macroscopic inspection of all samples.

3.3.3 Micro-computed tomography (micro-CT) evaluation of the explants. The samples harvested at the end of the LT study (12 weeks after implantation) were subjected to a micro-CT evaluation in order to analyse the 3D and 2D dimensions of the residual GG hydrogel matrices and eventually ingrown nerve tissue. Fig. 4 illustrates representative findings from the micro-CT evaluation of the explants, namely the explants' 3D and 2D images and the histograms that complement the histological images plus a correlating histological section after HE staining. In the AUTOG sample (positive control), the nerve tissue was clearly visible in the 3D image (enclosed in parafilm so that the samples would not dry) and corroborated by the histogram (Fig. 6A). No signs of new tissue formation were found in the NGC60:40 sample (Fig. 6B). The NGC50:50 sample's micro-CT images apparently showed some new tissue formation pointed out by the black arrow (Fig. 6C). In the NC25:75 sample, the brighter spots (white arrows) correspond to newly formed tissue, making the histogram more similar to the autologous graft (Fig. 6D). Despite the fact that NGC50:50 samples revealed the presence of some tissue, it did not appear to be as mature as the tissue detected in AUTOG and the NC25:75 samples.

3.3.4. Nerve histology for the detection of axonal regeneration and immunological reaction. The samples harvested 3 weeks after reconstruction were cut into cross-sections at certain distances from the proximal nerve end as exemplified in Fig. 5 (top row). HE and NF200 (data not shown) staining attested to the findings from the macroscopic evaluation: only 1 of the 4 NGC60:40 samples and 2 of the 4 NGC50:50 samples presented a certain degree of regrown tissue all along the conduit. The same was verified for 3 of the 4 NGC25:75
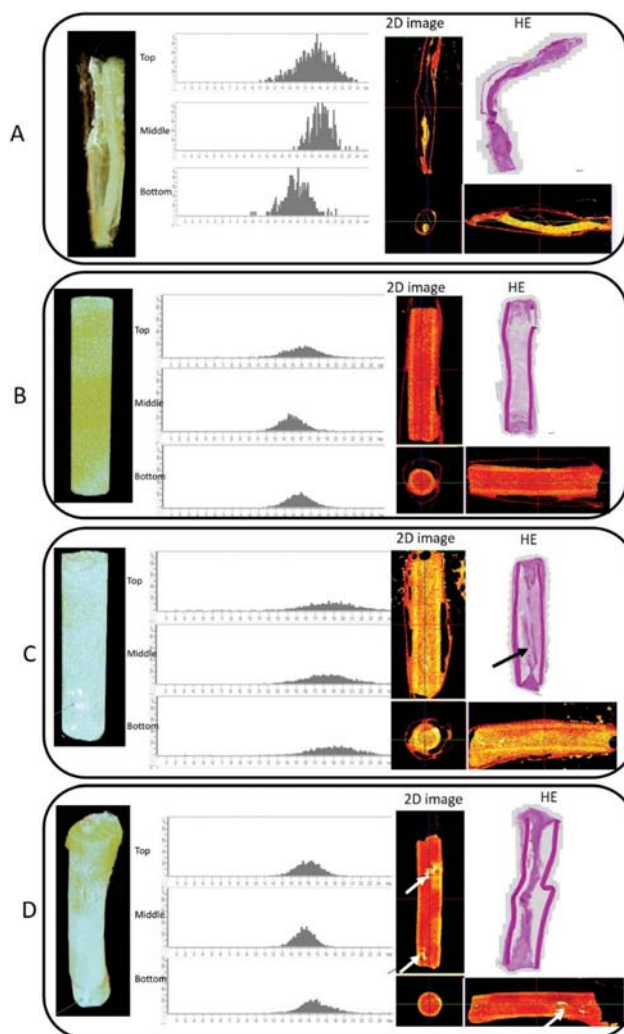

Fig. 4 Micro-computed tomography (micro-CT) evaluation of the explants 12 weeks after surgery and correlation to a corresponding HE stained histological section. For each sample, different characterization images are displayed in a panel, from left to right: 3D micro-CT reconstruction image, corresponding histograms concerning three areas of the conduit (top, middle and bottom), 2D micro-CT reconstructions (longitudinal sections in vertical and horizontal images and cross section in the quadratic box image) and histological sections (HE staining) in the upper left part of each panel. Note that in the case of the NGCs just the lumen area was selected as a Region of Interest (ROI) for the 3D reconstruction, thus excluding the chitosan tubes from the analysis. All samples were covered with parafilm to avoid water evaporation. (A) Positive control where the autologous nerve graft is visible and enclosed by parafilm; (B) the representative NGC60:40 sample shows no sign of cellular or tissue ingrowth in the NGC or the central GG matrix; (C) the representative NGC50:50 sample shows some tissue inside the NGC or the GG matrix (indicated by black arrows); (D) the representative NGC25:75 shows some tissue ingrowth (indicated by white arrows). Scale bar: 500 µm.

samples. HE representative microscopic pictures can be seen in Fig. 5, where black arrows point to regenerated tissue in every cross-section analysed (A, B, C and D). Histological images show that, regardless of the formulation, GG was still present inside the conduits (marked by asterisks and stained
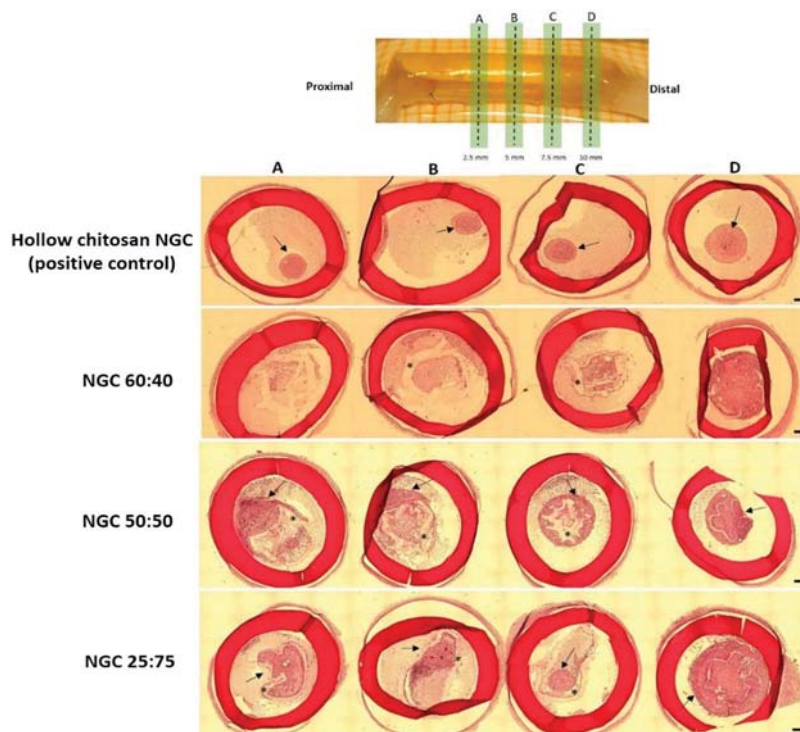
Fig. 5 Representative photomicrographs of the studied formulations after haematoxylin−eosin (HE) staining. Schematic representation of the cross-section positioning (top row, the example NGC is placed on scale paper with 1 mm intersections). Rows 2−4: HE stained cross-sections corresponding to chitosan hollow NGCs (positive control for the ST study) and NGCs filled with different GG freeze-dried formulations (NGC60:40, NGC50:50, NGC25:75) explanted 3 weeks after reconstruction. Black arrows point to regenerated tissue in the respective cross-sections. Asterisks are placed where residual GG is visible inside the NGCs. Scale bars: 200 µm.

in soft pink). Most of the residual GG material was detected in the NGC60:40 group samples. In general, re-growing tissue followed the longitudinal channels as guidance structures in NGC25:75 samples, where tissue regeneration was observed across the whole conduit. ESI Table 3† summarizes the results of the histological evaluation of tissue regrowth and axonal regeneration of all NGC samples harvested 3 weeks after reconstruction.

The samples explanted 6 and 12 weeks after the reconstruction were cut longitudinally in order to display the entire regeneration distance and tissue extension along the conduit. Representative pictures of such slides can be seen in Fig. 6. In all samples varying amounts of GG were still visible inside the NGC (marked by asterisks and stained in light pink). During analysis of both HE and anti-NF200 staining of sections corresponding to the 6 weeks' time point (upper row of Fig. 6), the impressions from the macroscopic evaluation were confirmed. Fig. 6A, corresponding to the positive control (hollow NGC), indicates the formation of a complete nerve bridge linking the two extremes of the lesion. In samples belonging to the NGC60:40 group, almost no cellular tissue or axons were detectable in the inner part of the conduit. Instead, NF-200 immunopositive axons were located along the tube wall, avoiding the GG as growth substrate (see an example in Fig. 6B). The appearance of samples belonging to the NGC50:50 group

was inconsistent. In general, less residual GG was present than in NGC60:40 samples (see an example in Fig. 6C) as 3/4 of the NGC25:75 presented an organized and almost intact tissue cable that almost extends to the distal nerve end. In these 3 encouraging samples, anti-NF200 stained regenerating axons (green fluorescence) were elongating from proximal to distal through the NGCs. An example of the NGC25:75 sample is shown in Fig. 6D. ESI Table 4† summarizes the results of the histological evaluation of tissue regrowth and axonal regeneration of all NGC samples harvested 6 weeks after reconstruction.

Histological findings corresponding to 12 weeks after nerve reconstruction (lower row of Fig. 6) match the ones from previous time points. The positive control in this case, an autotransplant, displayed a thick and complete nerve bridge between the original nerve ends that is mainly composed of NF200 immunopositive axons (Fig. 6A). In the NGC60:40 group the formation of new nerve tissue was scarce, and it showed pronounced fragmentation, indicating the complete absence of linearity (Fig. 6B). Samples from NGC50:50 displayed nerve trunk fragments irregularly found all along the nerve gap. This indicates the absence of a continuous nerve bridge with a consistent linear trajectory. Even in the samples that presented positive results in the electrodiagnostic recordings, the regenerated axons were not found to be aligned along
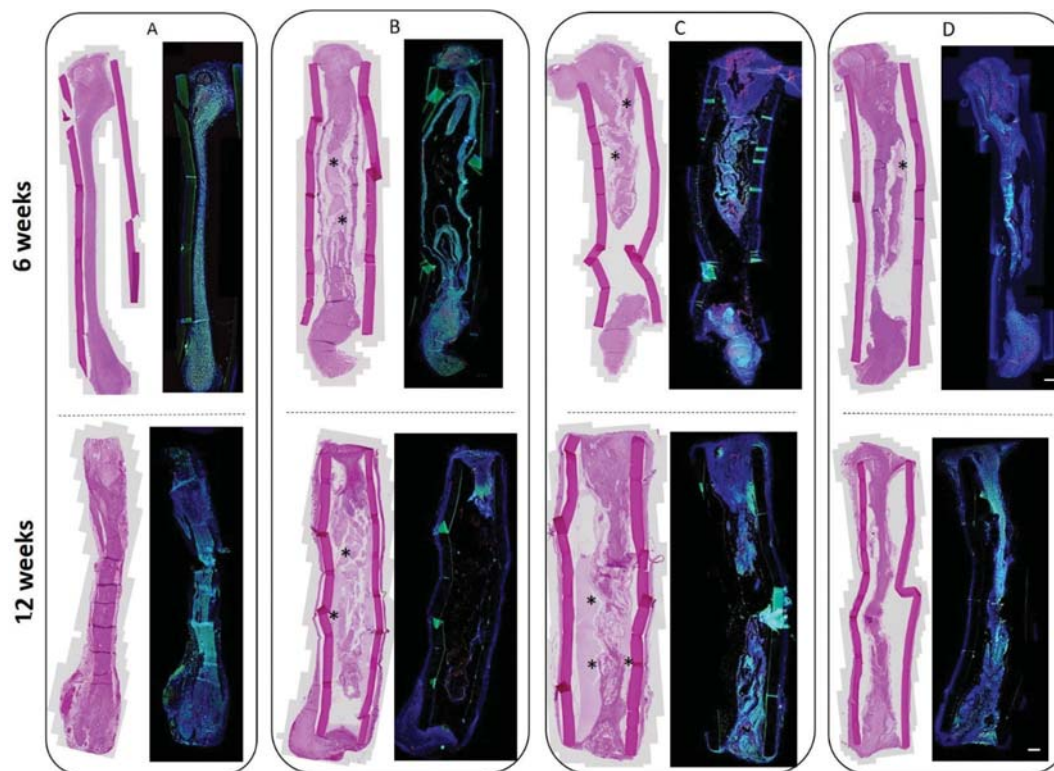
Fig. 6 Representative photomicrographs of histologically stained NGCs with GG fillings 6 and 12 weeks after reconstruction. Longitudinal sections for each sample after HE staining can be seen at left and the respective immunohistochemistry staining for NF200, ED1 and DAPI at right. (A) Positive control (hollow conduit at 6 weeks (ST study) and autologous nerve graft (LT study) at 12 weeks); (B) NGC60:40 sample; (C) NGC50:50; (D) NGC25:75. Proximal nerve end is on the top and distal nerve end is on the bottom. Asterisks mark the visible GG in light pink. Scale bars: 500 μm.

the longitudinal histological sections analysed (Fig. 6C). Almost all samples belonging to NGC25:75, namely the ones that presented positive results in the electrodiagnostic evaluation, display a thin but continuous nerve cable nearly connecting the two nerve ends along the histological sections analysed. Immunohistochemistry of these samples shows oriented axons along the conduit, invading the GG, which serves as a guiding cue, thus differing from the previous case. ESI Table S6† summarizes the results of the histological evaluation of tissue regrowth and axonal regeneration of all NGC samples harvested 12 weeks after reconstruction.

3.3.5. Nerve histology for the detection of neovascularization. Neo-vascularization was qualitatively evaluated by positive expression of two endothelial markers: CD31 (expressed on platelet and endothelial cell adhesion molecules, detected by green fluorescence) and CD34 (expressed on hematopoietic progenitor cells and the small vessel endothelium, detected in red fluorescence). Samples were collected from both, the ST and the LT, studies. The results of the immunohistochemical analysis show both blood vessel growth and blood cells proliferation. The presence of these vascular components is incremented as the amount of MA-GG in the formulations increases. Accordingly, NGC50:50 and NGC25:75 samples present an increasing neovascularization and it was perceptible that newly formed blood vessels accompany the newly

formed tissue throughout the conduit. This tendency was verified at all the studied time points (see Fig. 7 and ESI Tables S3–S5†).

3.3.6. Nerve morphometry of distal nerve segments. Nerve morphometry was performed on samples harvested in the LT study. For these analyses, only distal nerve segments originating from reconstructed nerves that have demonstrated muscle re-innervation during the final electrodiagnostic measurements were considered. More specifically, samples from the NGC50:50 and NGC25:75 groups were assessed, besides samples from the AUTOG positive control group (see Table S3†). Further control values were obtained from uninjured contralateral nerve segments. Although not significantly, it is obvious from Table S3† and Fig. 8 that the total number and density of NGC50:50 and NGC25:75 axons were decreased with respect to the values obtained from AUTOGs and increased with respect to healthy nerve values. However, AUTOGs, NGC50:50s, and NGC25:75 axon and fiber diameters, as well as myelin thickness, were reduced in distal segments from reconstructed nerves when compared to healthy nerves. Significantly reduced values were detected for the axon diameter, fibre diameter and myelin thickness between healthy and NGC25:75 distal nerve segments. Fig. 8 illustrates the previous quantitative results. It shows high resolution images of representative nerve semithin sections, stained
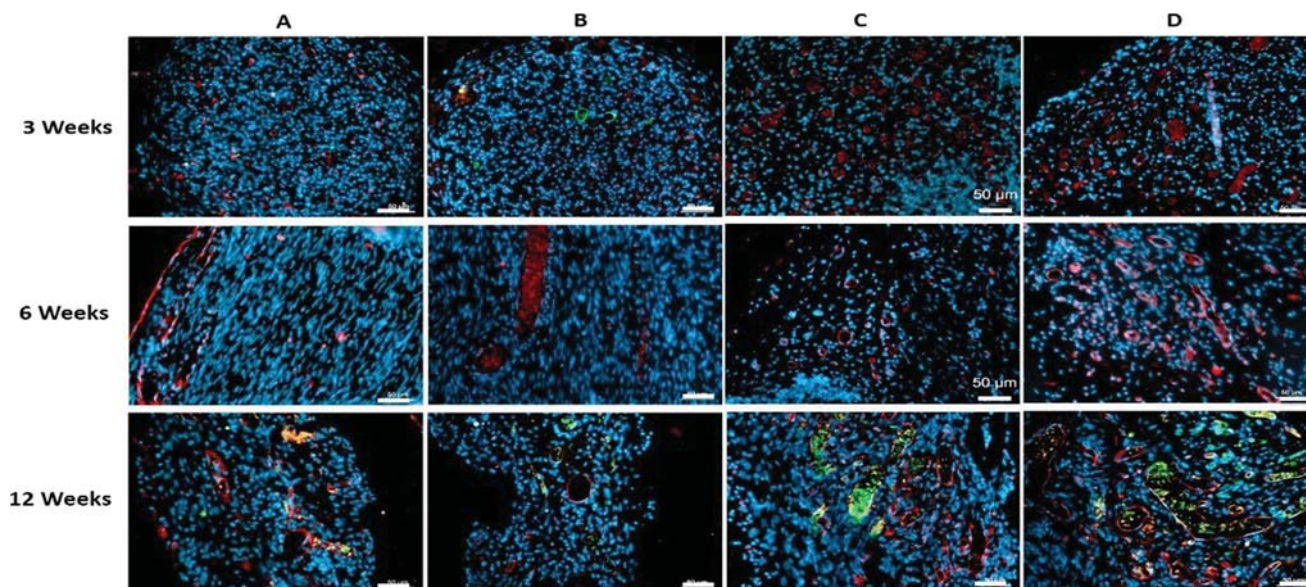
Fig. 7 Detection of neovascularization in the implanted formulations. Representative photomicrographs of immunohistologically stained sections corresponding to the studied formulations. Stains were performed for the detection of CD31 (green) and CD34 (red) after 3, 6 and 12 weeks post-reconstruction. Photomicrographs correspond to the central zone of the conduits. (A) Positive control (at 3 and 6 weeks is a hollow NGC and at 12 weeks is an ANG); (B) NGC60:40; (C) NGC50:50; (D) NGC25:75. Scale bars: 50 μm.
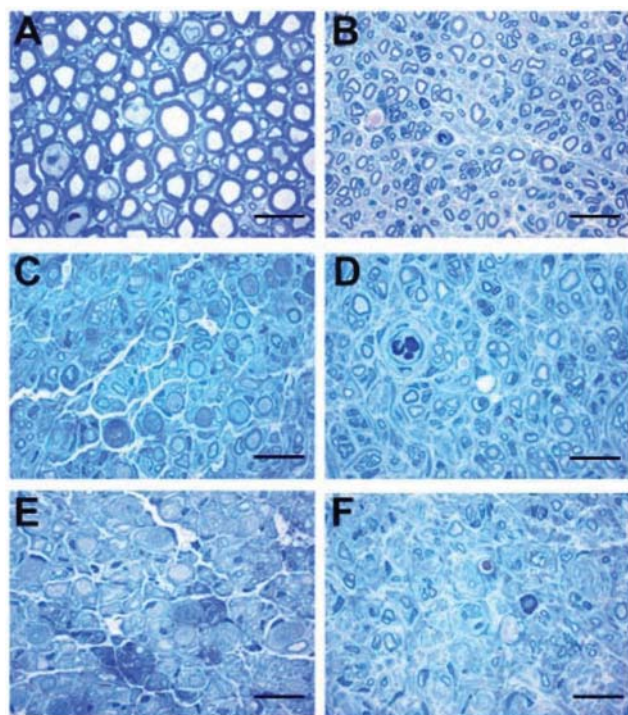

Fig. 8 Representative photomicrographs of myelinated axons visualized in distal peripheral nerve segments 12 weeks after reconstruction. High resolution images of representative semithin sections, stained with Toluidine blue, of nerve samples from (A) a healthy sciatic nerve and (B) that regenerated through an ANG; (C + D) NGC50:50 conduit, and (E + F) NGC25:75 conduit. Scale bars: 20 μm.

with Toluidine blue, from a healthy sciatic nerve (A), an AUTOG (B), an NGC50:50 conduit (C + D) and an NGC25:75 conduit (E + F).

4. Discussion

Experimental approaches for developing novel nerve guidance conduits (NGCs) lay an emerging focus on the creation of a three-dimensional endoneurial structure (resembling the Bands of Büngner).[34] The internal structures of luminal fillers of otherwise hollow NGCs should contribute to the regeneration process in different ways: (i) increase the intraluminal surface area, (ii) serve as supportive platforms to facilitate the extension of the regenerating axons, (iii) promote endogenous Schwann cell function, and (iv) eventually act as a drug delivery vehicle of pro-regenerative substances.[34,35] However, it should be kept in mind that the intraluminal structures may also negatively influence the regeneration process, for instance, by compromising the luminal permeability and penetrability or by affecting the NGC flexibility.[36] Gellan Gum (GG) was the material chosen as a luminal filler in this peripheral nerve repair (PNR) oriented study because of its biocompatibility, adequate physical properties, simply tunable features[37] and the fact that it has been largely explored within our group, in the context of other regenerative areas, with encouraging results.[38,39] The NGC shielding tube is made of chitosan with

approximately 5% degree of acetylation, which has already proved its PNR supporting properties.[9,20,40]

The rationale behind this experimental work is based on the fact that the hollow chitosan nerve guides approved as Reaxon® Nerve Guides fail to reconstruct peripheral nerve defects larger than 2.6 cm. Indeed, it is very difficult to bridge larger defects with bioartificial nerve grafts without the help of any type of cue, either physical or chemical, like the use of luminal fillers or growth factors, respectively.[41] In fact, allografts are the best option for longer gaps since they naturally provide the needed cues, like the native extracellular matrix present in the grafts but access to it is extremely difficult.[42] A luminal filler providing a valuable milieu for invading Schwann cells, good axonal guidance and induction of vascularization is suggested to lead to the development of such an implant. The GG freeze-dried hydrogel was chosen as a luminal filler in this study because of the ability to easily tune GG formulations and thereby influence its polymeric behaviour. Accordingly, different HA-GG : MA-GG blends gave rise to the diverse luminal fillers studied.[43] The evaluation of their characteristics was performed in a 10 mm sciatic nerve defect in order to select the most promising as a luminal filler for NGCs for future studies in longer gaps.

The first part of the study was dedicated to the production, physicochemical and *in vitro* testing of HA-GG : MA-GG freeze-dried hydrogels. The second part focused on the *in vivo* evaluation of diverse regeneration-associated parameters after the implantation of the developed NGCs.

A major constraint of traditional hydrogels as cell-instructive biomaterials for tissue engineering applications concerns the absence of cell adhesion motifs. For that reason, an intermediate step of freeze-drying was included in the process to obtain the final materials. This process transforms the specific spatial disposition of the hydrogel network. When the dry matrices are rehydrated with a cell suspension, cells become entrapped and are able to adhere and proliferate. This methodology offers the possibility of producing cell supporting matrices off-the-shelf that can be stored and quickly used.

Increasing attention is also being paid to the micro- and nanostructure of tissue engineering scaffolds for PNR.[35] Indeed, different strategies have been explored in this respect, *i.e.* the use of aligned fibres,[44] channels,[45] patterned surfaces[46] or electrical and magnetic fields.[47] In this respect, longitudinal channels were physically induced within our hydrogels by punching with a stainless-steel device.

SEM analysis demonstrated the micro-structure obtained in the final networks, where the freeze-drying induced porosity contrasts with the punched aligned porosity.

X-ray micro-computed tomography provides insight into how the GG scaffolds are oriented within the NGC. This technique captures images with spatial resolution in the micron domain, using X-ray beams to probe the interiors of opaque solid objects. Large pores and high % of porosity lead to minor trabecular thickness, which is translated into fragile and brittle systems in the dry state. Comparing the results,

there seems to be no relationship between the mean pore size or the % of porosity and the amount of HA-GG or MA-GG in the formulations.

These results were within the expected range, as we envisioned a highly porous and interconnected matrix inside the chitosan conduit, which would allow the growth of regenerating fibres, as well as guide them. Indeed, the method of production, freezing at −80 °C and subsequent freeze-drying, was selected because it allows great pores to be formed.[21]

However, despite the identically rigorous processing of freeze-dried hydrogels and NGCs, higher mean pore sizes and trabecular thickness were obtained in the second case. This indicates that the protector layer of the chitosan tube influences the formation of water crystals, probably by lowering the speed of freezing, ultimately altering the microstructure of the GG network inside the conduit. As a result, fewer pores are created, with reduced % of porosity and increased trabecular thickness. This effect can be also appreciated in the SEM images.

Concerning water uptake (WU), this parameter is related to the exchange of metabolic products and nutrients. Meanwhile, the weight loss (WL) is a parameter related to the biodegradation of the biomaterial. An optimized device for peripheral nerve reconstruction should remain intact until a proper invasion of repair Schwann cells occur, as these cells, together with invading perineurial cells, build the forefront of a regenerating nerve,[48] and then progressively degrade as the re-growing axons occupy new space.[49] Our *in vitro* results confirm that the formulations containing more MA-GG suffer from less swelling and degradation over time, as higher WU and WL were verified in H60:40, while the lowest values occurred for H0:100. On the one hand, this is probably because of the tighter matrix granted by the MA-GG when compared to native GG. In addition, methacrylate groups are hydrophobic in nature, thus impairing the interaction with water molecules.[50] On the other hand, higher percentages of HA-GG have been linked to faster degradation, due to the acyl group in its structure, which interferes with the gelling process. The resultant gels are weaker. Our results indicate that a relationship exists between the swelling ability and the degradation of the freeze-dried hydrogel materials. The formulations that take up more water are the ones that suffer more hydrolysis. This leads to the hypothesis that as water is taken up, it starts to break the trabeculae in the formulation microstructure.

Since to our knowledge GG systems have not been previously explored for PNR purposes, an immortalized Schwann cell line was used to evaluate the effect of the studied formulations on the performance of peripheral glial cells. The results indicate that a higher portion of MA-GG in the formulations is related to higher cell metabolic activity. This tendency has been previously observed for diverse cell types,[38,51] and is probably related to the stability and micro-structure of the matrices that MA-GG forms. An increased metabolic activity of invading Schwann cells is expected to be beneficial for the peripheral nerve regeneration process *in vivo*. In fact, nerve reconstruction

with formulations containing larger amounts of MA-GG, such as NGC25:75, resulted in better functional recovery than reconstruction with the other GG containing NGCs.

Summarizing the characterization results up to this point, the formulations containing larger amounts of HA-GG are likely to have a higher swelling rate, which is also likely to be accompanied by a faster degradation. Meanwhile, formulations with larger amounts of MA-GG offer the advantage of having a more positive influence over the cells in contact with them. *In vivo* experiments were designed in order to investigate how these characteristics balance each other once the formulations have been implanted into a peripheral nerve defect. Although the H0:100 formulation induced the highest cell metabolic activity, its low degradation rate seems inappropriate for PNR purposes. Accordingly, it was excluded from the *in vivo* tests in order to avoid unnecessary animal sacrifices.

In vivo results did not match the degradation rates of the isolated GG formulations *in vitro*. The *in vivo* tests showed that only small amounts of GG hydrogel residues were present in NGC25:75 (higher amounts of MA-GG) samples 6 and 12 weeks after nerve reconstruction. *Vice versa*, formulations containing larger amounts of HA-GG (NGC60:40) displayed larger residual amounts of non-degraded GG, which seemingly impaired regenerative tissue growth. Although isolated HA-GG formulations have higher degradation rate *in vitro*, certainly by hydrolysis mechanisms, it seems that other biological parameters influence the *in vivo* biodegradation of the studied formulations (*i.e.* specific enzymes such as amylase and lysozyme, cellular interaction or fluid infiltration),[50] leading to a faster clearance as the amount of MA-GG increases. The specific GG degradation mechanisms *in vivo* have not yet been identified yet.[24] WU also played an important role in the *in vivo* outcomes, as an excessive WU of the formulations containing increasing quantities of HA-GG has likely led to lumen-occlusion phenomena. The complete failure of nerve regeneration through NGC60:40 grafts could be a consequence of this phenomenon, allied to lower peripheral glial cell adhesion and axonal ingrowth. Following nerve transection, the process of regeneration is largely dependent on the activity of non-neuronal cells, such as macrophages or Schwann cells.[52] In fact, macrophages that are attracted to the injury site secrete substances that increase Schwann cell migration.[53] Beyond that, invading macrophages play a key role in eliminating both myelin and axonal debris, as well as in releasing a large number of axonal regeneration-related substances, including extracellular matrix (ECM) proteins, growth factors, cytokines and chemokines.[53] Consequently, the presence of such immune cells in the distal nerve segments following injury is important for the remodelling of the nerve. Nevertheless, an excessive and persistent amount of activated macrophages induced by the transplanted nerve guide material may lead to a progressive inflammatory response, which will have a detrimental effect on regeneration.[53] Both after 3, 6 and 12 weeks, NGC25:75 demonstrated a presence of activated ED1-immunopositive macrophages qualitatively comparable to that in the

positive control. These macrophages probably contributed to myelin and axonal clearance, a process that may be prolonged during weeks. In addition, macrophages were detected all along the lumen of NGC60:40 and NGC50:50 after 6 and 12 weeks of implantation. The fact that the formulations with larger HA-GG amount present more macrophages might suggest that this polymer is recognized as a foreign body by the host organism. Despite the good biocompatibility results shown by GG in other regenerative applications,[54] a foreign body reaction might originate due to the fact that these formulations were not degrading during the observation time. This finding points to the need of a faster degrading luminal filler material. Also, the authors hypothesize that the same formulations with larger HA-GG amount present great values of WU that impaired regeneration and that may also arouse some type of vigilante response by the host organism.[55]

The vascular net supplying peripheral nerves is very complex.[56] Furthermore, it is long known that angiogenesis is a crucial factor for a successful peripheral nerve regeneration across a critical length nerve gap and required for cell survival.[57] CD31 (PECAM-1; platelet/endothelial cell adhesion molecule-1) is a single chain type-1 transmembrane protein present in endothelial cells, which plays a key role in the interaction with adjacent CD34 (a single-chain transmembrane glycoprotein) expressing haematopoietic precursor cells or capillary endothelial cells. Both proteins are related to microvasculature formation.[58] After qualitative analysis, it seems that regardless of the GG formulation implanted within the NGCs, there was angiogenesis taking place. However, the presence of blood vessels (as well as the presence of erythrocytes within capillaries) seems to increase as the amount of MA-GG also increases within the formulations. This improved neoangiogenesis verified in NGC50:50 and NGC27:75 at all time points studied could have positively influenced the extent of functional recovery.

Interestingly, after 3 and 6 weeks, CD31 positive endothelial cells were not detected in any of the analysed sections, in contrast to CD34 that marked both blood vessels and red blood cells. However, by 12 weeks, both markers have been perceived, with CD34 marking mainly the endothelial cells in the walls of the newly generated blood vessels and CD31 identifying red blood cells. One possible explanation for this is that CD31 only identifies differentiated and mature cells, while CD34 already detects precursors of endothelial cells or not completely differentiated cells.[59]

The previously described micro-CT methodology is also a popular method to evaluate tissue engineering constructs,[60] human tissues[61] and animal tissues.[62] In a typical micro-CT image, relatively higher density structures appear brighter than structures with lower density. Soft tissues usually have a uniform density, and their internal structure cannot be discriminated with a conventional micro-CT method.[63] During the analysis of the explanted formulations, water, GG, and regenerated nerve tissue could not be discriminated properly in the wet explants since the densities of the soaked polymer and soft-tissue like nervous tissue are identical. The results of the current study indicate that NGC25:75 has better biological performance than

others, however, still not as good as the autologous graft. This information could not be retrieved from the 3D images reconstructions, but from the 2D cross and longitudinal sections and the histograms related to these images, in which density differences were detected pointing to the previous affirmation.

The initial macroscopic inspection of the explants after the *in vivo* observation time, matched the histological findings, such as the lumen-blocking properties of NGC60:40 and the pronounced induction of vascularization by NGC25:75. This, in turn, finds functional correlation with the results obtained from electrophysiological measurements, micro-CT analysis and nerve morphometry assessments in the distal nerve segments after 12 weeks post-surgery. Overall, the regeneration promoting properties of chitosan NGCs filled with the freeze-dried hydrogel GG scaffolds is significantly reduced in comparison to hollow chitosan NGCs for which in the same model in 69% of animals evocable CMAP signals were recorded from the tibialis anterior muscle 12 weeks after nerve reconstruction.[20] Muscle reinnervation detectable by electrodiagnostic procedures was, however, still found in some animals investigated throughout the current study. Nerve reconstruction with NGC60:40 completely prevented proper muscle reinnervation, while occurred to an increasing percentage in the NGC50:50 group and in the NGC25:75 group. Reinnervation of distal plantar interosseous muscles did, in the current study, only occur in the AUTOG group and was demonstrated, although to a lesser extent, also after implantation of hollow chitosan NGCs.[20] Morphometric analysis performed on nerve cross sections obtained distal to the grafts that resulted in functional recovery, confirmed the presence of regenerated myelinated axons. The fact that the overall results of the nerve morphometry indicate NGC50:50 as the eventually most promising formulation might be misleading, since despite two animals out of seven showed outstanding functional recovery, the remaining five showed no functional recovery at all. Consequently, it is probable that these outstanding results were due to any inter-individual variability between the groups of rats.

All together, these findings indicate that filling the lumen of chitosan NGCs with freeze-dried hydrogel GG scaffolds could not increase their peripheral nerve regeneration promoting properties, with results that do not outperform the positive controls used in both ST and LT studies (hollow chitosan tube and AUTOG, respectively). The concept of providing additional guidance structures inside the lumen of the NGCs is however still promising.[9] Indeed, the NGC25:75 implants showed a better performance than 5% degree of acetylation chitosan conduits containing NVR-Gel (composed of high molecular weight hyaluronic acid and laminin) as luminal filler. This study was performed by some of the authors of the present work, and proved that the previously indicated non-freeze dried hydrogels dramatically impaired nerve regeneration.[21] However, both of these studies demonstrate that a luminal filler such as an hydrogel or hydrogel-like structure present in the lumen might have detrimental effects in terms of nerve regeneration, since some obstruction is observed.

However, these results concerning the NGC25:75 highlight the potential of the GG presented during this experimental work, indicating the interest in continuing our research in this direction, further improving our NGC systems with methacrylated biomaterial.

5. Conclusions

This work demonstrates for the first time the innovative use of gellan gum freeze-dried hydrogels as luminal fillers for nerve guidance conduits intended for peripheral nerve reconstruction. The biomaterials have been evaluated *in vitro* before *in vivo* trials were initiated to define their short and long term potential to support peripheral nerve regeneration through chitosan nerve guides. The outcome of our studies demonstrates that the use of GG fillers did not result in improved nerve regeneration and that our system still has to be optimized. So far, the presence of such biomaterial in the lumen of the chitosan tubes might have negative effects in terms of nerve regeneration. The best results, however, have been achieved in the presence of larger amounts of MA-GG in the blending systems. The methacrylated material better supported axonal regeneration and increased vascularization, ultimately resulting in a certain degree of muscle re-innervation. Future attempts need to be focused on MA-GG formulations or peptide-modified GG for luminal fillers that are presented with lower concentrations of polymer or supplemented with supporting cells and/or regeneration promoting cues.

Conflicts of interest

The authors confirm that there are no known conflicts of interest associated with this publication and there has been no significant financial support for this work that could have influenced its outcome.

Acknowledgements

References

1 W. Daly, L. Yao, D. Zeugolis, A. Windebank and A. Pandit, *J. R. Soc., Interface*, 2012, **9**, 202–221.

2 V. Mukhatyar, L. Karumbaiah, J. Yeh and R. Bellamkonda, *Adv. Mater.*, 2009, **21**, 4670–4679.

3 M. Siemionow, M. Bozkurt and F. Zor, *Microsurgery*, 2010, **30**, 574–588.

4 T. E. Trumble and F. G. Shon, *Hand Clin.*, 2000, **16**, 105–122.

5 L. Korus, D. C. Ross, C. D. Doherty and T. A. Miller, *J. Neurol., Neurosurg. Psychiatry*, 2016, **87**, 188–197.

6 D. Grinsell and C. P. Keating, *BioMed Res. Int.*, 2014, **2014**, 698256.

7 K. Haastert-Talini, C. Mauritz, S. Chaturvedi and C. Grothe, *Nat. Protoc.*, 2007, **2**, 99–104.

8 F. Gonzalez-Perez, S. Cobianchi, S. Geuna, C. Barwig, T. Freier, E. Udina and X. Navarro, *Microsurgery*, 2015, **35**, 300–308.

9 C. Meyer, L. Stenberg, F. Gonzalez-Perez, S. Wrobel, G. Ronchi, E. Udina, S. Suganuma, S. Geuna, X. Navarro, L. B. Dahlin, C. Grothe and K. Haastert-Talini, *Biomaterials*, 2016, **76**, 33–51.

10 T. M. Dinis, R. Elia, G. Vidal, Q. Dermigny, C. Denoeud, D. L. Kaplan, C. Egles and F. Marin, *J. Mech. Behav. Biomed. Mater.*, 2015, **41**, 43–55.

11 D. Santos, G. Giudetti, S. Micera, X. Navarro and J. del Valle, *Brain Res.*, 2016, **1636**, 93–106.

12 L. M. Marquardt, X. Ee, N. Iyer, D. Hunter, S. E. Mackinnon, M. D. Wood and S. E. Sakiyama-Elbert, *Tissue Eng., Part A*, 2015, **21**, 2852–2864.

13 S. M. Klein, J. Vykoukal, D. P. Li, H. L. Pan, K. Zeitler, E. Alt, S. Geis, O. Felthaus and L. Prantl, *Plast. Reconstr. Surg.*, 2016, **138**, 132–139.

14 Y. Sowa, T. Kishida, T. Imura, T. Numajiri, K. Nishino, Y. Tabata and O. Mazda, *Plast. Reconstr. Surg.*, 2016, **137**, 318e–330e.

15 X. Gu, F. Ding and D. F. Williams, *Biomaterials*, 2014, **35**, 6143–6156.

16 S. Kehoe, X. F. Zhang and D. Boyd, *Injury*, 2012, **43**, 553–572.

17 T. M. Dinis, R. Elia, G. Vidal, Q. Dermigny, C. Denoeud, D. L. Kaplan, C. Egles and F. Marin, *J. Mech. Behav. Biomed. Mater.*, 2015, **41**, 43–55.

18 Q. Ao, A. Wang, W. Cao, L. Zhang, L. Kong, Q. He, Y. Gong and X. Zhang, *J. Biomed. Mater. Res., Part A*, 2006, **77**, 11–18.

19 S. Gnavi, C. Barwig, T. Freier, K. Haastert-Talini, C. Grothe and S. Geuna, *Int. Rev. Neurobiol.*, 2013, **109**, 1–62.

20 K. Haastert-Talini, S. Geuna, L. B. Dahlin, C. Meyer, L. Stenberg, T. Freier, C. Heimann, C. Barwig, L. F. Pinto, S. Raimondo, G. Gambarotta, S. R. Samy, N. Sousa, A. J. Salgado, A. Ratzka, S. Wrobel and C. Grothe, *Biomaterials*, 2013, **34**, 9886–9904.

21 C. Meyer, S. Wrobel, S. Raimondo, S. Rochkind, C. Heimann, A. Shahar, O. Ziv-Polat, S. Geuna, C. Grothe and K. Haastert-Talini, *Cell Transplant.*, 2016, **25**, 159–182.

22 J. Silva-Correia, A. Gloria, M. B. Oliveira, J. F. Mano, J. M. Oliveira, L. Ambrosio and R. L. Reis, *J. Biomed. Mater. Res., Part A*, 2013, **101**, 3438–3446.

23 S. J. Chang, Y.-T. Huang, S.-C. Yang, S.-M. Kuo and M.-W. Lee, *Carbohydr. Polym.*, 2012, **88**, 684–689.

24 H. Lee, S. Fisher, M. S. Kallos and C. J. Hunter, *J. Biomed. Mater. Res., Part B*, 2011, **98**, 238–245.

25 M. T. Cerqueira, L. P. da Silva, T. C. Santos, R. P. Pirraco, V. M. Correlo, A. P. Marques and R. L. Reis, *Tissue Eng., Part A*, 2014, **20**, 1369–1378.

26 T. E. L. Douglas, M. Pilarz, M. Lopez-Heredia, G. Brackman, D. Schaubroeck, L. Balcaen, V. Bliznuk, P. Dubruel, C. Knabe-Ducheyne, F. Vanhaecke, T. Coenye and E. Pamula, *J. Tissue Eng. Regener. Med.*, 2017, **11**, 1610–1618.

27 C. A. Carmona-Moran, O. Zavgorodnya, A. D. Penman, E. Kharlampieva, S. L. Bridges Jr., R. W. Hergenrother, J. A. Singh and T. M. Wick, *Int. J. Pharm.*, 2016, **509**, 465–476.

28 F. I. Boni, F. G. Prezotti and B. S. Cury, *Drug Dev. Ind. Pharm.*, 2016, **42**, 1283–1290.

29 C. Grothe, C. Meisinger, J. Holzschuh, K. Wewetzer and P. Cattini, *Brain Res. Mol. Brain Res.*, 1998, **57**, 97–105.

30 M. Karnovsky, *J. Cell Biol.*, 1965, **27**, 137–138.

31 A. Feria-Velasco and M. J. Karnovsky, *Arch. Invest. Med.*, 1970, **1**, 201–220.

32 O. Schultze, *Z. Wiss. Mikrosk.*, 1910, **27**, 465–475.

33 S. C. Huelsenbeck, A. Rohrbeck, A. Handreck, G. Hellmich, E. Kiaei, I. Roettinger, C. Grothe, I. Just and K. Haastert-Talini, *Neurotherapeutics*, 2012, **9**, 185–198.

34 A. Faroni, S. A. Mobasseri, P. J. Kingham and A. J. Reid, *Adv. Drug Delivery Rev.*, 2015, **82–83**, 160–167.

35 R. V. Bellamkonda, *Biomaterials*, 2006, **27**, 3515–3518.

36 O. A. Carballo-Molina and I. Velasco, *Front. Cell. Neurosci.*, 2015, **9**, 13.

37 L. R. Stevens, K. J. Gilmore, G. G. Wallace and M. in het Panhuis, *Biomater. Sci.*, 2016, **4**, 1276–1290.

38 J. Silva-Correia, J. M. Oliveira, S. G. Caridade, J. T. Oliveira, R. A. Sousa, J. F. Mano and R. L. Reis, *J. Tissue Eng. Regener. Med.*, 2011, **5**, e97–107.

39 L. P. da Silva, M. T. Cerqueira, R. A. Sousa, R. L. Reis, V. M. Correlo and A. P. Marques, *Acta Biomater.*, 2014, **10**, 4787–4797.

40 S. Wrobel, S. C. Serra, S. Ribeiro-Samy, N. Sousa, C. Heimann, C. Barwig, C. Grothe, A. J. Salgado and K. Haastert-Talini, *Tissue Eng., Part A*, 2014, **20**, 2339–2349.

41 S. Mobini, B. S. Spearman, C. S. Lacko and C. E. Schmidt, *Curr. Opin. Biomed. Eng.*, 2017, **4**, 134–142.

42 D. N. Brooks, R. V. Weber, J. D. Chao, B. D. Rinker, J. Zoldos, M. R. Robichaux, S. B. Ruggeri, K. A. Anderson, E. E. Bonatz, S. M. Wisotsky, M. S. Cho, C. Wilson, E. O. Cooper, J. V. Ingari, B. Safa, B. M. Parrett and G. M. Buncke, *Microsurgery*, 2012, **32**, 1–14.

43 G. Khang, S. K. Lee, H. N. Kim, J. Silva-Correia, M. E. Gomes, C. A. Viegas, I. R. Dias, J. M. Oliveira and R. L. Reis, *J. Tissue Eng. Regener. Med.*, 2015, **9**, 265–275.

44 S. K. Vimal, N. Ahamad and D. S. Katti, *Mater. Sci. Eng., C*, 2016, **63**, 616–627.

45 R. Sridharan, R. B. Reilly and C. T. Buckley, *J. Mech. Behav. Biomed. Mater.*, 2015, **41**, 124–135.

46 A. Mobasseri, A. Faroni, B. M. Minogue, S. Downes, G. Terenghi and A. J. Reid, *Tissue Eng., Part A*, 2015, **21**, 1152–1162.

47 Y. Li, P. S. Wang, G. Lucas, R. Li and L. Yao, *Stem Cell Res. Ther.*, 2015, **6**, 41.

48 J. S. Belkas, M. S. Shoichet and R. Midha, *Neurol. Res.*, 2004, **26**, 151–160.

49 M. B. Steed, V. Mukhatyar, C. Valmikinathan and R. V. Bellamkonda, *Atlas Oral Maxillofac. Surg. Clin.*, 2011, **19**, 119–130.

50 D. F. Coutinho, S. V. Sant, H. Shin, J. T. Oliveira, M. E. Gomes, N. M. Neves, A. Khademhosseini and R. L. Reis, *Biomaterials*, 2010, **31**, 7494–7502.

51 J. W. Nichol, S. Koshy, H. Bae, C. M. Hwang, S. Yamanlar and A. Khademhosseini, *Biomaterials*, 2010, **31**, 5536–5544.

52 P. Chen, X. Piao and P. Bonaldo, *Acta Neuropathol.*, 2015, **130**, 605–618.

53 A. D. Gaudet, P. G. Popovich and M. S. Ramer, *J. Neuroinflammation*, 2011, **8**, 110–110.

54 J. Silva-Correia, B. Zavan, V. Vindigni, T. H. Silva, J. M. Oliveira, G. Abatangelo and R. L. Reis, *Adv. Healthcare Mater.*, 2013, **2**, 568–575.

55 J. M. Anderson, A. Rodriguez and D. T. Chang, *Semin. Immunol.*, 2008, **20**, 86–100.

56 M. Lehmann, M. A. Konerding and M. Blank, in *Peripheral Nerve Lesions*, ed. M. Samii, Springer Berlin Heidelberg, Berlin, Heidelberg, 1990, pp. 149–153, DOI: 10.1007/978-3-642-75611-5_22.

57 G. Penkert, W. Bini and M. Samii, *J Reconstr. Microsurg.*, 1988, **4**, 319–325.

58 A. M. Pisacane, F. Picciotto and M. Risio, *Cell. Oncol.*, 2007, **29**, 59–66.

59 H. Nagatsuka, K. Hibi, M. Gunduz, H. Tsujigiwa, R. Tamamura, T. Sugahara, A. Sasaki and N. Nagai, *J. Oral Pathol. Med.*, 2005, **34**, 70–76.

60 I. F. Cengiz, J. M. Oliveira and R. L. Reis, *J. Mater. Sci.: Mater. Med.*, 2017, **28**, 129.

61 H. Pereira, S. G. Caridade, A. M. Frias, J. Silva-Correia, D. R. Pereira, I. F. Cengiz, J. F. Mano, J. M. Oliveira, J. Espregueira-Mendes and R. L. Reis, *Osteoarthr. Cartil.*, 2014, **22**, 1271–1281.

62 J. Cardeira, P. J. Gavaia, I. Fernandez, I. F. Cengiz, J. Moreira-Silva, J. M. Oliveira, R. L. Reis, M. L. Cancela and V. Laize, *Sci. Rep.*, 2016, **6**, 39191.

63 R. Mizutani and Y. Suzuki, *Micron*, 2012, **43**, 104–115.